Kinetics of the coherent order-disorder transition in Al_3Zr

Laurent Proville* and Alphonse Finel
Laboratoire d'Etude des Microstructures, ONERA–CNRS, Boîte Postale 72, 92322 Châtillon Cedex, France
(Received 31 January 2001; published 10 July 2001)

Within a phase field approach which takes the strain-induced elasticity into account, the kinetics of the coherent order-disorder transition is investigated for the specific case of Al_3Zr alloy. It is shown that a microstructure with cubic $L1_2$ precipitates appears as a transient state during the decomposition of a homogeneous disordered solid solution into a microstructure with tetragonal DO_{23} precipitates embedded into a disordered matrix. At low enough temperature, favored by a weak internal stress, only $L1_2$ precipitates grow in the transient microstructure preceding nucleation of the DO_{23} precipitates that occurs exclusively at the interface of the solid solution with the $L1_2$ precipitates. Analysis of microstructures at nanoscopic scale shows a characteristic rod shape for the DO_{23} precipitates due to the combination of their tetragonal symmetry and their large internal stress.

DOI: 10.1103/PhysRevB.64.054104 PACS number(s): 61.66.Dk, 68.35.Rh, 64.60.Cn, 64.60.My

I. INTRODUCTION

Macroscopic properties of materials depend to a large extend on the microstructures they present at a mesoscopic scale. For the case of alloys the most efficient way to control the formation of microstructures is by phase transformations. Well known prototypes are the γ-γ' superalloys, such as Ni-Al (see Ref. 1). The microstructure of such binary alloys consists of stable ordered domains, dispersed in a disordered fcc matrix. The symmetry of the ordered domains is called $L1_2$: the atoms of the minority species are placed at the corner of the fcc motif and the atoms of the majority species occupies the center of the faces of the same motif.

The macroscopic properties are controlled by the size of precipitates, their spatial distribution, and their ability to resist to coarsening. In this context, we present a theoretical study of the dynamics of microstructures in an aluminum based alloy, namely, Al-Zr.

In this system, for low enough concentration, the equilibrium ordered structure is the tetragonal DO_{23} phase. Its motif is obtained from the $L1_2$ structure with antiphase boundaries in (100) directions with the period of 4. In Al-Zr the cubic $L1_2$ phase is known to be metastable at all temperature T. This is confirmed by *ab initio* electronic calculations at $T=0$ K (Refs. 6,7) which show that the energy difference between $L1_2$ and DO_{23} is about 0.863×10^8 J/m^3 (or 9.1 meV/atom), in favor of DO_{23}. However, the lattice misfit of DO_{23} with respect to pure Al is significantly larger than $L1_2$. Hence, the interplay between the chemical energy and, for coherent microstructures, the elastic energy may induce various precipitation processes.

The aim of the present work is to investigate the decomposition processes and to analyze the resulting microstructures at mesoscopic scale. We use a phase field approach, where the incoherent chemical energy is represented by a Ginzburg-Landau free energy supplemented by a strain-induced elastic energy, in the form proposed by Khachaturyan.[2–4] Using numerical simulations, we show that the coherent elastic strain favors the $L1_2$ phase at low Zr concentration and low temperature and in that range the kinetics generates $L1_2$ rather than DO_{23} precipitates. If the coherent elastic interactions are not included, only DO_{23} precipitates nucleate.

Our simulations prove that one may obtain metastable $L1_2$ phase in specific conditions that correspond to the experimental conditions leading to a $L1_2$ microstructure. The lifetime of that microstructure may be infinite compared to the simulation time, provided the temperature is not too high. Once the $L1_2$ precipitates have grown at sufficiently low temperature, the system may be brought to a higher temperature, where no $L1_2$ would nucleate if the system had been quenched directly to that temperature. If the already developed $L1_2$ microstructure is aged again at higher temperature, then the DO_{23} precipitation starts and DO_{23} precipitates nucleate exclusively along the interfaces between $L1_2$ inclusions and the matrix. Once DO_{23} precipitates are formed, they grow and consume the $L1_2$ domains. The latest transformation cannot be reversed with decreasing temperature.

In Sec. II, the general principles of the kinetic model are presented. In Sec. III, we outline how the microelasticity contribution can be included into the model. The implementation of the phase transition kinetics, the results obtained and their interpretation are given in Sec. IV. Conclusions and perspectives are drawn in Sec. V.

II. GINZBURG-LANDAU FUNCTIONAL

Our mesoscopic method is a time-dependent Ginzburg-Landau kinetics driven by a functional with two parts: first a Ginzburg-Landau functional that includes the chemical interactions and second a strain-induced elastic energy.

The explicit form of the Ginzburg-Landau (GL) free energy is imposed by symmetry rules. The first step consists in identifying the long range order (LRO) parameters that represent the ordered phases we want to study. In the present situation, we should introduce the LRO parameters of DO_{23} and $L1_2$. Nevertheless, to simplify the writing of the GL free energy, we choose to replace the DO_{23} LRO parameters with the DO_{22} ones as these phases are both tetragonal. What differs between them is only the periodicity of the antiphase

boundaries that is 2 for DO_{22} instead of 3 for DO_{23}. As our aim is not to investigate the competition between the latter phases, our description only requires to capture the tetragonality of the possible stable ordered phase.

The $L1_2$ phase is simple: it consists in three independent parameters η_1, η_2, η_3 which correspond to the amplitudes of the three waves that contribute to $L1_2$. The waves correspond to the three vectors of the reciprocal space $K_1=(100)$, $K_2=(010)$, $K_3=(001)$, respectively. If the microstructure consists only in $L1_2$ domains embedded into a disordered fcc matrix, the local concentration $c(R)$ would be given by

$$c(R)=c_0(R)+\sum_{j=\{1,2,3\}}\eta_j(R)\exp(i2\pi K_j R), \qquad (2.1)$$

where the quantities $c_0(R)$ and $\eta_j(R)$ vary slowly in space. For a DO_{22} structure, the probability $c(R)$ to find a atom Zr at position R can be written as follows:

$$c(R)=c_0(R)+\sum_{j=\{1,2,3\}}\eta_j(R)\exp(i2\pi K_j R)+\gamma_j(R)\exp(i2\pi Q_j R)+\gamma_j^*(R)\exp(-i2\pi Q_j R), \qquad (2.2)$$

where γ_j^* is the complex conjugate of the amplitude parameter γ_j and $Q_1=(1/2\,1\,0)$, $Q_2=(0\,1/2\,1)$, and $Q_3=(1\,0\,1/2)$ blong to the reciprocal cubic lattice. This choice is not unique but is sufficient. For example, $(1/2\;0\;1)$ can be replaced by $(1/2\;1\;0)$; each index j corresponds to a possible orientation of the tetragonal transformation yielding DO_{22}. For each of the three orientational variants there are four translational variants. For example, for a perfect DO_{22} phase with the orientation $j=1$, one has four translational variants defined, respectively, by $\gamma_1^*=\eta_1$, $\gamma_1^*=-\eta_1$, $\gamma_1^*=-i\eta_1$, $\gamma_1^*=i\eta_1$. For simplicity we drop the complex variants. It does not affect the description as there are still two translation variants for each orientation of the DO_{22} phase.

We note that the state $\gamma_j=0$ and $\eta_j\neq 0$ for $j=1,2,3$ leads to a density $c(R)$ that describes a $L1_2$ phase. A perfect $L1_2$ implies that the three (100)-type waves have the same amplitude. As $L1_2$ preserves the cubic symmetry there is no orientational variant but only four translational variants.

We now develop a uniform Landau functional as a function of $\{c_0,\eta_j,\gamma_j\}$. The terms of this analytical function $f_L(c_0,\eta,\gamma)=F_0.\hat{f}_L$ are selected to fit with the symmetry of the fcc lattice, that is each term must be invariant under any operation of the fcc symmetry group. Formally there is no other rule to realize a polynomial expansion but the simplest form is probably the best. In practice, other conditions (see below) must be satisfied. We propose the following adimentional functional:

$$\hat{f}_L=A_n(c_0-c_1)^n+\frac{A_2}{2}(c_2-c_0)\sum_i\eta_i^2-A_3\eta_1\eta_2\eta_3+\frac{A_4}{4}\eta_i^4+K_3\gamma_i^2\eta_i+\frac{K_4}{2}\sum_{j=i\pm1}\gamma_i^2\eta_j^2+\frac{B_2}{2}(c_2-c_0)\gamma_i^2-\frac{B_4}{4}\gamma_i^4+\frac{B_4'}{2}\sum_{j=i\pm1}\gamma_i^2\gamma_j^2+\frac{B_6}{6}\gamma_i^6, \qquad (2.3)$$

where order parameters indices are written modulo 3. The hat symbol points out the adimensional quantities: here $\hat{f}_L$ is an adimensional free energy density. The sets of coefficients $\{A_j\}$, $\{B_j\}$, $\{K_j\}$, and $\{c_1,c_2\}$ should vary with the temperature but are chosen as constant parameters for simplicity. The first term in the right hand side of Eq. (2.3) is the disorder contribution as it does not depend on the order parameters. The power n of that term may have two values $n=n_+=2$ and $n=n_-=8$ whether $c_0>c_1$ or not. We introduce that property to adjust the topology of the Landau functional with both experimental and *ab initio* measurements as described below. The continuity of the first and second derivatives of the Landau functional are preserved which is sufficient for the present case.

The next three terms with A_2,A_3,A_4 amplitudes are the contribution of the star $(1\,0\,0)$. The four last terms associated with B_2,B_4,B_4',B_6 are the contribution of the concentration waves $\{Q_i\}_i$. The expansion to the sixth order is required to obtain the linear stability of both DO_{22} and $L1_2$ phases for the same range of concentration. The $\{K_4\}$ and $\{B_4'\}$ coefficients couple concentration waves with different orientations. They control the amplitude of the potential barrier between the minima that correspond to ordered phases. The K_3 term is the amplitude of the coupling between the waves that belong to the same orientational DO_{22} variant, (K_i,Q_i) and equivalents.

In fact, the precise form of the Landau functional term by term has not a direct influence on the mesoscopic microstructure providing that the functional is globally invariant with respect to the space group of the fcc lattice. The important ingredients are the excess free-energy associated with interfaces and long-range elastic interactions between domains. Therefore, we keep the lowest order coupling term between the LRO parameters associated with (K_i,Q_i) , i. e., terms of the form $\gamma_i^2\eta_i$.

The energy scale is fixed by the F_0 coefficient. The parameters of the adimensional free-energy density $\hat{f}_L(c_0,\eta,\gamma)$ are adjusted to fit the required qualitative thermodynamical properties. In Fig. 1 is plotted versus concentration c_0 the free energy density $F_0\hat{f}_L$ minimized with respect to the LRO parameters. The three types of minima correspond to the disordered phase, the DO_{23} (or DO_{22}) and $L1_2$ structures. The common tangent constructions determine the regions where ordered phases may coexist with the solid solution. The concentrations $c_{DO_{23},a}$ and $c_{DO_{23},b}$ are the limit of the region where coexist both disordered solid solution with the DO_{23} phase. Similar quantities can be determine for the coexistence of solid solution with $L1_2$ phase: $c_{L1_2,a}$ and

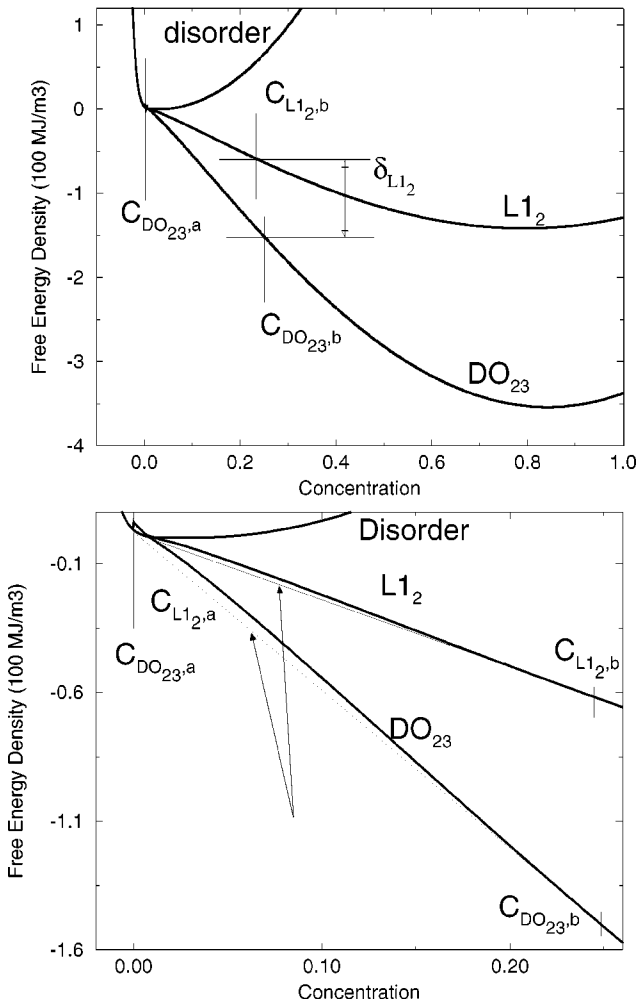

FIG. 1. Uniform free energy density versus concentration, with minima corresponding to the phases DO_{23} and $L1_2$ and the solid solution. On the right, magnification of the common tangent constructions (pointed by arrows).

$c_{L1_2,b}$. The concentration $c_{L1_2,a}$ and $c_{DO_{23},a}$ are the solubility limit of the $L1_2$ and DO_{23} phases, respectively.

In a nonuniform system, the order parameters η_i and γ_i and the local concentration c_0 are spatially dependant. Within a phase-field approach, these parameters vary continuously thought the system. The energy excess due to interfaces is expressed as a continuous Hamiltonian of the parameter fields and their first derivatives. To the lowest order, this leads to the following Ginzburg-Landau (GL) free energy density:

$$f_{GL}=F_0\left[\hat{f}_L(c_0,\eta,\gamma)+\left\{\lambda_c|\nabla c_0|^2+\sum_i \lambda_\eta\nabla^2\eta_i + \lambda_\gamma\nabla^2\gamma_i\right\}\right], \tag{2.4}$$

where the λ coefficients are the weight of the gradient terms. Total energy is given by $F_{GL}=\int f_{GL}dV$. For the numerical implementation, we introduce a discrete space which is a cubic sublattice with unit cell of linear size d. This length must be large enough to justify our continuous approach and define the scale of one pixel in our simulations. The total free energy can be expressed as a discrete sum $F_{GL}=d^3\Sigma_L f_{GL}$ where L represents the set of the sublattice nodes.

We now describe the physical requirement we use to adjust the Ginzburg-Landau functional. First, c_{L1_2a} and $c_{DO_{23}a}$ (see Fig. 1) are the solubility limit of both $L1_2$ and DO_{23} if each phase is supposed to coexist alone with solid solution. The $c_{DO_{22}a}$ is given by the uncoherent phase diagram and c_{L1_2a} has been estimated by the measure of the lattice parameter of the solid solution by x ray using Vegard's law.[5] For Zr at temperature $T=425\,^\circ$C, $c_{DO_{22}a}=0.0308$ and $c_{L1_2a}=0.0426$ at. %.[5]

Second, to analyze the competition between the metastable $L1_2$ and stable DO_{23} structures during the precipitation and aging processes, the free energy difference between both phases is an important quantity. In order to estimate this difference we refer to the theoretical studies of the formation energies obtained by *ab initio* electronic structure methods.[6–9] In Ref. 6, it is found that ground-state of Al_3Zr is indeed DO_{23}, and its structure is stabilized by the relaxation of the atomic positions inside the elementary cell. The difference of energy between $L1_2$ and DO_{23} is found to be $\delta_{L1_2}=0.863\times10^8$ J/m^3. In term of a phase field approach, this corresponds to an uncoherent energy at zero temperature. We assume that for low enough temperature, the free energy difference δ_{L1_2} do not vary strongly. Therefore, the *ab initio* quantity δ_{L1_2} is used to fix the scale F_0 of the free energy [Eq. (2.4)] through the relation $F_0=\delta_{L1_2}/\hat{\delta}_{L1_2}$ where $\hat{\delta}_{L1_2}$ is the energy difference between the corresponding $L1_2$ and DO_{23} minima of the adimentional free energy $\hat{f}_L$ which has been minimized taking into account the conservation of the c_0 concentration parameter that yields the common tangent construction (see Fig. 1).

Finally, another very important feature of the GL functional is the excess of energy of the interface between solid solution and precipitates, noted I_o with $o=\{L1_2,DO_{23}\}$. These quantities play a role in nucleation and growth process. The interface energy of ordered precipitates in the solid solution can be measured experimentally at very low supersaturation. The Lifshitz-Slyozov-Wagner theory[10] gives the interface energy as a function of the diffusion coefficient which is physically measured. Unfortunately the few we found in literature (see Ref. 5) about such a measurement is not satisfactory as the interface energy measured for $L1_2$ precipitates I_{L1_2} is hundred times larger than the usual values. Thus we choose to estimate I_{L1_2} to a value of 10 mJ/m^2 which is the order of magnitude of interface energies measured in aluminum compounds. As we did not find measurement in literature concerning interface energy of DO_{23} precipitates $I_{DO_{23}}$, we choose for $I_{DO_{23}}$ a similar value to that of I_{L1_2} because there is no physical reason these two quantities to differ by an order of magnitude. We adjust the interface energies of the ordered phases $\{o\}$ of the adimensional GL functional $\hat{I}_o$ such as $F_0 d\hat{I}_o=I_o$. It implies $\hat{I}_{DO_{23}}/\hat{I}_{L1_2}$

$=I_{DO_{23}}/I_{L1_2}$. With some difficulties, we managed to adjust the GL functional such that both $\hat{I}_{\mathrm{DO}_{23}}$ and $\hat{I}_{L1_2}$ have the same order of magnitude. The F_0 being fixed by the second criteriion stated previously, it imposes $d=I_o/\hat{I}_o\hat{\delta}_{L1_2}/\delta_{L1_2}$ so we can define the scale of our simulation. In order to investigate the nanometer scale we choose $d=1$ nm, then the $\hat{f}$ functional must verify $\hat{I}_o/\hat{\delta}_{L1_2}\approx 0.26$. The only way we found to satisfy the previous criteria is to introduce the nonsymmetric power $n_{\pm}$ for the term $(c-c_1)^{n_{\pm}}$ in the GL functional. Finally we obtain $c_{\mathrm{DO}_{22}a}=0.0308\%$, $c_{L1_2a}=0.5\%$, and $F_0 d\hat{I}_{L1_2}=8$ mJ/m^2, $F_0 d\hat{I}_{\mathrm{DO}_{22}}=9$ mJ/m^2. The pixel of our simulation represents a cube of size $d=0.5$ nm.

III. MICROELASTICITY CONTRIBUTION TO FREE ENERGY

As described in Ref. 4, the elastic energy E_{el} is calculated assuming that the local strain (ϵ_{kl}) induces a relaxation that is calculated by setting a small volume dV of the bulk to the mechanical equilibrium. It is supposed that the time needed to reach the mechanical equilibrium is negligible compared to the typical diffusive time of the ordering process. The key point of the phase field theory for alloys is that the stress free strain tensor can be expressed as a function of the local LRO parameters and local concentration $c_0(R)$.

The geometrical operation to transform a cubic unit cell of the solid solution with lattice parameter $\overline{a}$ into the cubic unit cell of the $L1_2$ phase with lattice parameter a_{L1_2} is given by the tensor

$$\epsilon_{kl}^{L1_2}=\delta_{kl}(a_{L1_2}-\overline{a})/\overline{a}, \tag{3.1}$$

where δ_{kl} is the unity tensor. The lattice parameter a_{L1_2} has been measured for a perfect $L1_2$ phase,[5] i.e., with stoichiometry 0.25 at. % $rmZr$ and $\overline{a}$ is extrapolated from the lattice parameter a_0 of pure aluminum Al, using Vegard's law.

We note $a_{\mathrm{DO}_{23}}$ and $b_{\mathrm{DO}_{23}}$ the lattice parameters of the tetragonal DO_{23} phase at stoichiometry 0.25 at. % Zr. The geometrical operation to transform a cubic unit cell of the solid solution into the tetragonal elementary cell of the DO_{23} phase is given by the tensor $\epsilon_{kl}^{\mathrm{DO}_{23}}(p)$ if the orientational variant corresponds to the association of the (K_p,Q_p) waves with $p=1,2\,or\,3$: the cell is dilatated in either (100), (010), or (001) direction. Here we choose as an example the orientational variant associated to (K_1,Q_1) and the cubic unit cell is dilated in the direction (100) so as $b_{\mathrm{DO}_{23}}>\overline{a}>a_{\mathrm{DO}_{23}}$.

$$\epsilon^{\mathrm{DO}_{23}}(1)=\frac{b_{\mathrm{DO}_{23}}-\overline{a}}{\overline{a}}\begin{pmatrix}1&0&0\\0&t&0\\0&0&t\end{pmatrix}, \tag{3.2}$$

where $t=(a_{\mathrm{DO}_{23}}-\overline{a})/(b_{\mathrm{DO}_{23}}-\overline{a})$. Tensors $\epsilon_{kl}^{\mathrm{DO}_{23}}(2)$ and $\epsilon_{kl}^{\mathrm{DO}_{23}}(3)$ derive from $\epsilon_{kl}^{\mathrm{DO}_{23}}(1)$ by permutation of the diagonal coefficients. For the general expression of the local strain, we propose the following form (see Ref. 4):

$$\epsilon_{kl}^{0}(R)=\epsilon_{kl}^{00}(0)\psi_0(R)+\sum_{p=1}^{3}\epsilon_{kl}^{00}(p)\psi_p(R), \tag{3.3}$$

where $\psi_p(R)=[\gamma_p(R)]^2$, and $\psi_0(R)=[c_0(R)-\overline{c}]$. The tensor coefficients $\epsilon_{kl}^{00}(p)$ are chosen in a such way that $\epsilon_{kl}^{0}(R)=\epsilon_{kl}^{L1_2}$ if a relaxed $L1_2$ inclusion is at the position R and $\epsilon_{kl}^{0}(R)=\epsilon_{kl}^{\mathrm{DO}_{23}(p)}$ if a DO_{23} inclusion is in the same position with the orientational variant p. The Eq. (3.3) is rewritten in a compact form $\epsilon^0(R)=\Sigma_{p=0}^{3}\epsilon^{00}(p)\psi_p(R)$ where the p indice varies now from 0 to 3. The strain-induced elastic energy can be computed following the model presented in Ref. 11 which gives

$$E_{el}=\frac{1}{2}\sum_{p,q}\int[B_{pq}]\tilde{\psi}_p^*\tilde{\psi}_q dK^3, \tag{3.4}$$

where $\tilde{\psi}_p$ is the Fourier transform of the function ψ_p. There

$$B_{p,q}(K)=\lambda_{ijkl}\epsilon_{kl}^{00}(p)\epsilon_{ij}^{00}(q)-b_{pq}(K)$$

and $b_{pq}(K)=\sigma_{i,j}^{00}(p)\ K_i\ G_{jk}\ K_l\ \sigma_{kl}^{00}(q)$ where λ_{ijkl} is the elastic tensor and $\sigma_{ij}^{00}(p)=\lambda_{ijkl}\epsilon_{kl}^{00}(p)$. The tensor G_{jk} is the elastic Green function. The tensor λ_{ijkl} is assumed to be homogeneous in space and the simulations are realized with elastic coefficients of aluminum.[11]

IV. KINETICS OF THE PHASE TRANSFORMATION

The total energy is given by the sum $F=F_{GL}+E_{el}$ [Eqs. (2.4) and (3.4)]. At mesoscopic scale, the kinetics of the phase transition is well described by a phase field method (see Ref. 12). In the context of a phase field approach, the local composition c_0 is a conservative order parameter and thus its time evolution is driven by the Cahn-Hilliard equation

$$\frac{\partial c_0(R,t)}{\partial t}=L_c\triangle\frac{\delta F}{\delta c_0(R,t)}+\upsilon^c(R,t) \tag{4.1}$$

and for the nonconservative LRO parameters the kinetic is given by

$$\frac{\partial\eta_j}{\partial t}=-L_\eta\frac{\delta F}{\delta\eta_j}+\upsilon^{\eta_j}(R,t), \tag{4.2}$$

$$\frac{\partial\gamma_j}{\partial t}=-L_\gamma\frac{\delta F}{\delta\gamma_j}+\upsilon^{\gamma_j}(R,t), \tag{4.3}$$

where υ's are stochastic terms. To simulate thermal fluctuations, it is useful to introduce the Langevin noise which consists in assuming a white space-time noise for the stochastic terms and no cross-correlation between each other. Numerically, the random functions υ's are implemented with a gaussian probability density.[13]

The set of Eqs. (4.1)–(4.3) is the so-called time-dependant Ginzburg-Landau equation[4] and they can be derived from the microscopic Onsager equation with respect to

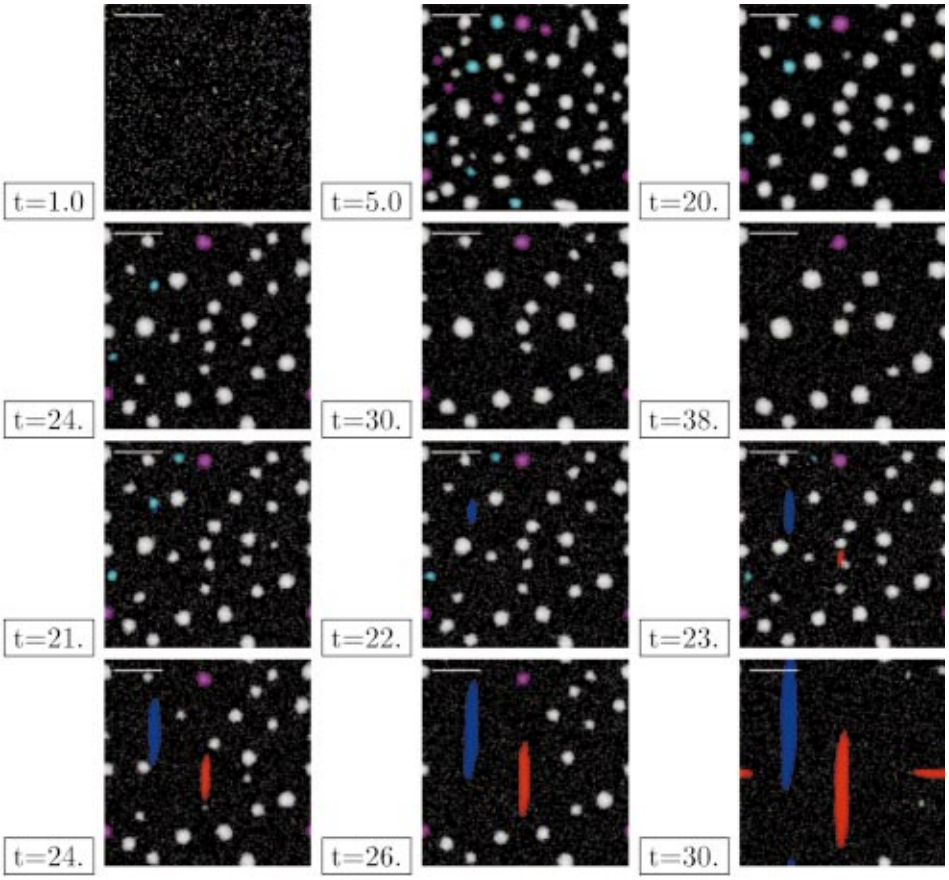

FIG. 2. (Color) Simulation of aging for $\bar{c}=2$ at. % Zr, $T=425$ K (first row). At time $t=20$, T is increased at $T=848$ K (second row) and at $T=1100$ K (third and fourth rows). Note that the DO_{23} (red and blue) precipitates grow at the interface of $L1_2$ precipitates (pale) with the solid solution with rod shape. White lines at top left corner of the pictures represent 15 nm and indicate the (1 0 0) direction.

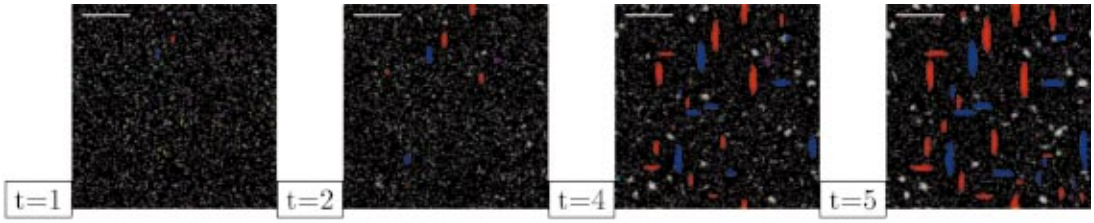

FIG. 3. (Color) Isothermally aging at $T=850$ K and $\bar{c}=2$ at. % Zr.

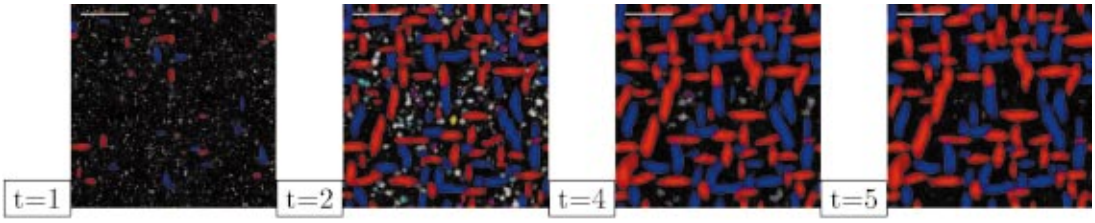

FIG. 4. (Color) Isothermally aging at $T=1100$ K, $\bar{c}=3$ at. % Zr.

the occupation probability of the solute atoms.[2] Numerically, for simplicity, we choose $L_\gamma = L_\eta = L_c = 1$. So in order to deduce the approximative time unit of our simulations, our numerical time must be divided by the numerical value of the diffusion coefficient. The Langevin noise provides a very primitive description of the thermal fluctuations. All though it is the simplest and the less controversal way to implement the temperature in the simulation.

Equations (4.1)–(4.3) are integrated on a system that is invariant along the z axis to save computation time. The initial state of the system is a uniform solid solution at concentration $c_{L1_2,a} < c_0 = \overline{c} < 0.25$ and all the set of LRO parameters are set to zero value, which represents an unstable disordered phase. The initial time of our simulation can be considered as an instantaneous quenching of the material.

To represent the microstructures we choose to color the DO_{23} precipitates with either blue or red depending on their translational variant. The four translational variants of $L1_2$ are allocated to four other paler colors. The disordered phase is colored with black. The gray scale is sufficient to distinguish the different types of precipitates if the translational variants are forgotten. In Figs. 2–4, we present the dynamics of the phase transition from disordered solid solution to a microstructure with ordered precipitates embedded into a disordered matrix. The different sequences are realized for different average compositions $\overline{c}$ and different temperatures T.

First, one notes the specific rod shape of the DO_{23} precipitates. The tetragonal symmetry combined with a large misfit $(b_{DO_{23}} - \overline{a})/\overline{a}$ which involves a large intrinsic stress is well known to induce such a pattern.[4] On the very last picture of Fig. 2 the facets of the DO_{23} inclusions correspond to the habit planes with orientation of around 20° with respect to the (1 0 0) directions. For any couple of external variables, namely the temperature T and the composition $\overline{c}$ the late stage of the kinetics is a microstructure which contains exclusively the DO_{23} precipitates embedded in a disordered matrix. Nevertheless $L1_2$ structures may appear in the early regime of the dynamics (see Fig. 3). As the $L1_2$ ordered precipitates involve a weak misfit $(a_{L1_2} - \overline{a})/\overline{a}$ compared to $(b_{DO_{23}} - \overline{a})/\overline{a}$, their shape is spherical. These spherical inclusions nucleate only at low temperature T and low Zr concentration $\overline{c}$. At low enough values of T and for saturation $\overline{c}$ close enough from the solubility limit, the microstructure contains exclusively the $L1_2$ precipitates inside the solid solution. Since the $L1_2$ phase is metastable, any grain of this phase should not resist to thermal fluctuations and thus no $L1_2$ precipitates should grow in the microstructure. It is actually what is observed if the elastic energy E_{el} is neglected in our simulations. However, in the limit of low Zr saturation, the kinetics of the transition drives the system to a transient $L1_2$ microstructure which is favored by its intrinsic stress which is weaker than that of DO_{23}. If the temperature T is not too high, i.e., $T < T_{L1_2} \approx 500$ K (see Fig. 2), the $L1_2$ precipitates can even grow by consuming the very few solute atoms contained in the disordered matrix. This implies that the solid solution becomes poor in solute and therefore the nucleation of DO_{23} precipitates is no longer possible in the disoredered matrix. In fact, if temperature is lower than T_{L1_2}, the $L1_2$ microstructure may survive for a time much longer than the computation time. Nevertheless, a gradual increase of the temperature reveals the process of nucleation of the DO_{23} precipitates (see Fig. 2). A remarkable result is that nucleation of the stable phase occurs at the interface of the $L1_2$ precipitates with the solid solution where the local concentration c_0 is high enough. One note that the preferential growth of DO_{23} precipitates occurs at temperature higher than T_{L1_2} that demonstrates the robusness of the metastable $L1_2$ microstructure with respect to thermal fluctuations.

Similar simulations at larger saturation $\overline{c}$ show that both the DO_{23} and $L1_2$ precipitates nucleate and may coexist in the microstructure (see Fig. 4). In that range of $\overline{c}$, the DO_{23} inclusions can nucleate at places different from $L1_2$ precipitates because the solute atoms have not been consumed by the growth of $L1_2$ inclusions. Once saturation of the solid solution is locally dried up, the DO_{23} precipitates grow to the expense of the $L1_2$ grains via the solute diffusion throught the matrix. Then the persistent $L1_2$ precipitates are localized relatively far from the DO_{23} grain. For a given temperature, if the average concentration $\overline{c}$ is increased again, the grains with different phases nucleate in neighboring regions of the supersaturated solid solution and the DO_{23} inclusions absorbe the Zr matter of $L1_2$ inclusions.

One remark on Figs. 2–4 that the orientational variant of DO_{23} which is combination of waves (K_3, Q_3) is inhibited. It is because the precipitates with such variant cannot relax their elastic energy because of z invariance. Qualitatively it is not a problem as there are still two orientational variants for the DO_{23} phase.

V. CONCLUSION AND PERSPECTIVE

The present paper treats of the specific case of the interplay between the $L1_2$ metastable phase and the DO_{23} ordered ground-state during the order-disorder transition in Al_3Zr alloy. It is proved that for a sufficiently low temperature and weak solute saturation the metastable phase nucleates before the stable phase. It is the result of the dynamics of the phase transition that is deeply influenced by the microelasticity induced by the strain of precipitates. The metastable ordered phase with a weak internal stress may be favored with respect to the ordered ground state which induces a much larger strain. The strain-induced elasticity may play a role at the early regime of the dynamics of the phase transition. Furthermore, depending on external variables, temperature and composition, we found different kinetics for the vanishing of the $L1_2$ precipitates. At low temperature and low saturation of solute, the DO_{23} precipitates grow preferentially at the interfaces of $L1_2$ inclusions with solid solution. At higher temperature or equivalently higher Zr saturation, the DO_{23} precipitates nucleate into the solid solution. Once DO_{23} precipitates have nucleated, they grow at expense of the $L1_2$ structure that disappears. Actually, such phenomena have not

yet been observed experimentally. With this respect, the phase field method can be considered as a predictive method, though experimental confirmation is now required. On that trail, microscope analysis are programmed in the Laboratoire d'Etude des Microstructures (ONERA).

It is well known experimentally that the $L1_2$ microstructure has better mechanical properties than DO_{23}. As the $L1_2$ is metastable, the degradation of the mechanical properties with increasing temperature cannot be avoid. Nevertheless our results allow to hope that it is possible to increase the robusness of the $L1_2$ microstructure playing with elastic interaction. We expect our study will contribute to the understanding of precipitates formation and to improve the control of the alloys synthesis. To that purpose, the phase field method we use, can be extended for other alloys with similar phase transition as Ti_3Al or Pd_3V.

Finally our calculations are only valid for coherent sample at the nanometer scale. It is possible to investigate noncoherent effect introducing dislocations in the phase-field method as it is discribed in both Refs. 14 and 15. It is of great interest to perform such simulation in the case of Al_3Zr where discontinuous precipitations and dislocations modify strongly the precipitation process[16,17] and play an important role in macroscopic properties of materials.

*Present address: Groupe de Physique des Solides, UMR 7588–CNRS, Universités Paris 6 et Paris 7, 2 pl. Jussieu 75251, Paris Cedex 05, France.

[1] A.B. Kamara, A.J. Ardell, and C.N.J. Wagner, Metall. Mater. Trans. A **27** 2888 (1996).

[2] A.G. Khachaturyan, *Theory of Structural Transformations in Solids* (Wiley-Interscience, New York, 1983).

[3] L.Q. Chen and A.G. Khachaturyan, Phys. Rev. Lett. **70**, 1477 (1993).

[4] Yunzhi Wang, L.Q. Chen, and A.G. Khachaturyan, in *Computer in Material Science*, Vol. 308 of NATO ASI Series, edited by H.O. Kirchner, L.P. Kubin, and V. Pontikis (Plenum, New York, 1996), p. 325.

[5] M.S. Zedalis and M.E. Fine, Metall. Mater. Trans. A **17**, 2187 (1986).

[6] C. Amador, J. Hoyt, B. Chakoumakos, and D. de Fontaine, Phys. Rev. Lett. **74**, 4955 (1995).

[7] Jian-hua Xu and A.J. Freeman, Phys. Rev. B **40**, 11 927 (1989); **41**, 12 553 (1990).

[8] A.E. Carlsson and P.J. Meschter, J. Mater. Res. **4**, 1060 (1989).

[9] M. Alatalo, M. Weinert, and R.E. Watson, Phys. Rev. B **57**, 2009 (1998).

[10] I.M. Lifshitz and V.V. Slyozov, J. Phys. Chem. Solids **19**, 35 (1961); C. Wagner, Z. Elektrochem. **65**, 581 (1961).

[11] D. Lazarus, Phys. Rev. **76**, 545 (1949).

[12] J.D. Ganton, M.M. San, and P.S. Mahni, *Phase Transitions and Critical Phenomena*, edited by C. Domb and J.L. Lebowitz (Academic, New York, 1983), Vol. 8, p. 269.

[13] URL http://www.ulib.org/webRoot/Books/NumericalRecipes/bookf90.html.

[14] Y.U. Wang, Y.M. Jin, A.M. Cuitio, and A.G. Khachaturyan, Acta Mater. **49**, 1847 (2001).

[15] D. Rodney and Finel, in *Influences of Interface and Dislocation Behavior on Microstructure Evolution*, MRS Symposia Proceedings No. 652 (Materials Research Society, Warrendale, PA, in press).

[16] E. Nes, Acta Mettal. **20**, 499 (1972); E. Nes and H. Billdal, *ibid.* **25**, 1039 (1977).

[17] N. Ryum, Acta Mettal. **17**, 269 (1969).